Detectable Impact of Local and Remote Anthropogenic Aerosols on the 20th Century Changes of West African and South Asian Monsoon Precipitation

Journal of Geophysical Research: Atmospheres

RESEARCH ARTICLE
10.1029/2017JD027711

Key Points:
- Impact of anthropogenic aerosols by source region is detected on 20th century West African and South Asian monsoon precipitation changes
- South Asian/West African monsoon precipitation changes are dominated by aerosols from South Asia/North America and Europe
- Changes in West Africa are related to a shift in circulation; those in South Asia are associated with a weakening of the monsoon circulation

Supporting Information:
- Supporting Information S1

Correspondence to:
S. Undorf,
s.undorf@ed.ac.uk

Citation:
Undorf, S., Polson, D., Bollasina, M. A., Ming, Y., Schurer, A., & Hegerl, G. C. (2018). Detectable impact of local and remote anthropogenic aerosols on the 20th century changes of West African and South Asian monsoon precipitation. *Journal of Geophysical Research: Atmospheres*, *123*. https://doi.org/10.1029/2017JD027711

Received 8 SEP 2017
Accepted 15 APR 2018
Accepted article online 8 MAY 2018

Detectable Impact of Local and Remote Anthropogenic Aerosols on the 20th Century Changes of West African and South Asian Monsoon Precipitation

S. Undorf[1], D. Polson[1], M. A. Bollasina[1], Y. Ming[2], A. Schurer[1], and G. C. Hegerl[1]

[1]School of GeoSciences, The University of Edinburgh, Edinburgh, UK, [2]NOAA Geophysical Fluid Dynamics Laboratory, Princeton, NJ, USA

Abstract Anthropogenic aerosols are a key driver of changes in summer monsoon precipitation in the Northern Hemisphere during the 20th century. Here we apply detection and attribution methods to investigate causes of change in the West African and South Asian monsoons separately and identify the aerosol source regions that are most important for explaining the observed changes during 1920–2005. Historical simulations with the GFDL-CM3 model are used to derive fingerprints of aerosol forcing from different regions. For West Africa, remote aerosol emissions from North America and Europe (NAEU) are essential in order to detect the anthropogenic signal in observed monsoon precipitation changes. The changes are significantly underestimated in the model, however. While natural (volcanic) forcing seems to also play a role, the dominant contribution is found to come from aerosol-induced changes in the interhemispheric temperature gradient and associated meridional shifts of the Intertropical Convergence Zone. For South Asia, in contrast, changes in observed monsoon precipitation cannot be explained without local emissions. Here the findings show a weakening of the monsoon circulation, driven by the increase of remote NAEU aerosol emissions until 1975, and since then by the increase in local emissions offsetting the decrease of NAEU emissions. The results show that the aerosol forcing from individual emission regions is strong enough to be detected over internal variability. They also underscore the importance of the spatial pattern of global-aerosol emissions, which is likely to continue to change throughout the expected near-future decline in global emissions.

1. Introduction

Monsoon precipitation is vital for more than two thirds of the world's population as a critical resource for economy, agriculture, water resources, and ecosystems throughout the monsoon region. Observational records have shown that monsoon rainfall underwent substantial decadal scale and even longer-term variations during the past 150 years (Gallego et al., 2015; Turner & Annamalai, 2012), sometimes resulting in catastrophic impacts for these vulnerable societies. An issue of particular interest and concern is to ascertain the extent to which human activities have contributed to driving these changes. This is important for enabling the management and mitigation of the impacts of future monsoon variations associated with climate change.

Anthropogenic aerosols have emerged as an important driver of global and regional climate, partially offsetting the impact of greenhouse gases (GHGs; e.g., Tett et al., 2002). By scattering and absorbing incoming solar radiation, aerosols reduce the radiation reaching the surface, thus cooling the surface while heating the atmosphere and increasing its vertical stability (Ming & Ramaswamy, 2009). In addition to this direct effect (and associated adjustments and feedbacks), aerosols can alter precipitation through complex interactions with cloud microphysical processes (indirect effects; Rotstayn & Lohmann, 2002): By acting as cloud condensation nuclei, aerosols increase the cloud albedo (Twomey, 1977) as well as the cloud lifetime by precipitation suppression (Albrecht, 1989). Large uncertainties are associated with aerosol emissions and background concentrations (Carslaw et al., 2013), and global climate models (GCMs) differ in their parameterization of aerosol effects (Wilcox et al., 2015). While they also show large discrepancies in their simulated regional to global response to aerosol forcing (Kasoar et al., 2016), GCMs are still a useful tool to infer the impact of aerosols on climate.

At hemispheric scale, increased aerosol emissions from human activities predominantly located in the Northern Hemisphere have been linked to a southward shift of the Intertropical Convergence Zone (ITCZ) during the twentieth century, altering tropical precipitation patterns (Ackerley et al., 2011; Hwang et al., 2013; Rotstayn et al., 2015). Regionally, a number of studies have suggested anthropogenic aerosols to have played a key role in modulating the Northern Hemisphere summer monsoon precipitation (Polson et al., 2014), driving or contributing to the reduction in monsoon precipitation in West Africa and the Sahel (Dong, Sutton, et al., 2014; Held et al., 2005) and Asia (Bollasina et al., 2011; Guo et al., 2015; Lau et al., 2006; Li et al., 2015, 2016) during the twentieth century. This is in stark contrast with the expected impact from increased GHG emissions, which would instead lead to increased monsoon precipitation (e.g., Guo et al., 2015). Yet the existence of counteracting effects between GHGs and aerosols can make it difficult to *robustly* distinguish the influence of one from another (Wang et al., 2016; Xie et al., 2013), especially at regional scale.

In contrast to GHGs, aerosols have short residence times in the atmosphere, which results in a heterogeneous spatial distribution closely following the pattern of emission sources (see supporting information Figure S2 in Wilcox et al., 2015). Throughout the twentieth century, the fraction of global-aerosol loading due to Asian sources has been growing and eventually outweighed the hitherto dominant contribution from North American and European sources (Lamarque et al., 2010). This gradual emission shift has important implications not only for regional climate, since the aerosol impact can extend beyond the emission regions via, for example, fast atmospheric circulation adjustments, to affect the large-scale, if not, hemispheric-wide climate (Boucher et al., 2013). In particular, precipitation in different regions might respond differently to aerosol forcing depending on aerosol source region. Modeling studies suggest a role for both local and nonlocal aerosols in weakening monsoons in Asia (Cowan & Cai, 2011; Dong et al., 2015; Guo et al., 2015) and West Africa (Dong, Sutton, et al., 2014), though local aerosol emissions are suggested to be predominantly responsible for the drying of the South Asian monsoon (Bollasina et al., 2014; Ganguly et al., 2012; Guo et al., 2016; Salzmann et al., 2014). Some other studies looked at the effect of the simultaneous increase of Asian emissions and decrease of North American and European emissions (Tsai et al., 2016), but the relative influence of aerosols from different regions on the various monsoon systems still remains largely unclear.

In this study, we extend earlier work (Polson et al., 2014) to analyze the West African and South Asian summer monsoons in isolation and contrast the impact brought about by aerosols emitted from the major extratropical and tropical source regions on precipitation changes in each monsoon system. We make use of ensemble simulations with the U.S. National Oceanic and Atmospheric Administration (NOAA) Geophysical Fluid Dynamics Laboratory (GFDL) coupled climate model version 3 (CM3). This model was chosen because it treats aerosol-cloud interactions and aerosol indirect effects explicitly (Donner et al., 2011), simulates key climatological features of the Asian monsoon more realistically than most other models (Sperber et al., 2013), and is one of the models with smallest biases in summer low-level clouds over West Africa, a key factor modulating monsoon precipitation there (Hannak et al., 2017). In the simulations, emissions from individual source regions are kept at preindustrial levels while evolving everywhere else. We derive fingerprints of precipitation changes in the form of time series and use detection and attribution methods to determine whether — and to what extent — the different forcing fingerprints contribute to the changes or whether the latter could be explained by internal variability alone. We additionally investigate the corresponding changes in the large-scale atmospheric temperature and circulation in order to shed light on the dynamical changes driving the detected precipitation signals. The remainder of the manuscript is organized as follows: section 2 presents the observational and model data used and describes the analysis methods, including an overview of the detection and attribution methodology. The results from the analysis of spatiotemporal changes in precipitation over the West African and South Asian monsoon regions are shown in section 3. Section 4 investigates the underlying physical mechanisms associated with the precipitation changes, highlighting the links with variations in the large-scale atmospheric circulation. Discussion and concluding remarks follow in section 5.

2. Data and Methods

2.1. Observations and Models

Two monthly gridded observational data sets are used to calculate the mean summer (June–September, JJAS) precipitation anomalies in the West African and South Asian monsoon regions for 1920–2005: the Climate Research Unit data set, CRUTS3.24 (CRU; Harris et al., 2014), and the Global Precipitation Climatology Centre data set (GPCC; Schneider, Becker, et al., 2014). Both data sets make use of the same raw station data

but apply different methodologies to derive the gridded products. Both may contain artifacts caused by inhomogeneities such as variable number of stations per grid box over time (Beck et al., 2005) and infilling. In particular, the methodology of CRU gives greater temporal fidelity while GPCC uses a larger number of stations. The analysis focuses on the West African and South Asian monsoons, which are two of the largest components of the global monsoon system and located entirely within the tropics. They have been shown to be interconnected at decadal time scales (e.g., Feudale & Kucharski, 2013). The availability of extensive station records in these regions dating back to the 1920s increases the detectability of the forced signals. Changes are examined for the JJAS months as they encompass the entire monsoon season throughout the domain. For the analysis of the latitudinal position of the ITCZ, we use additional satellite data from the Global Precipitation Climatology Project (GPCP; Adler et al., 2003).

The model data consist of a set of four twentieth century experiments with the 1°×2.5° GFDL-CM3 model. Each experiment is a three-member ensemble, forced with different combinations of time-evolving anthropogenic aerosol emissions (i.e., all other forcings are kept at preindustrial levels). Three of the ensembles have global time-varying historical emissions with the exception of those from (1) North America and Europe (NoNAEU), (2) South Asia (NoSA), or (3) China (NoCH) fixed at preindustrial levels. The fourth experiment has historical aerosol emissions for South Asia only and preindustrial aerosol emissions in the rest of the world (SAonly; see Figure S1 in the supporting information). These experiments are used to derive response patterns to regional-aerosol emissions and are interpreted in the context of additional simulations with global time-varying anthropogenic aerosol (AA), greenhouse gas (GHG), and natural (volcanic and solar; NAT) forcing individually (three members each), as well as their combination in the all-forcing ensemble (ALL, five members). Taking regional emission changes away in the NoNAEU, NoSA, and NoCH simulations rather than exclusively including them, as well as the complementarity of the SAonly and NoSA cases, reduces the potential problem of nonlinearities in the interactions when simulating the response to regional aerosols separately (see Figure S2 and section 2.3). Note that dust emissions from climatologically prescribed sources are a function of wind speed and direction. We also make use of simulations from the Coupled Model Intercomparison Project (CMIP) 5 archive (see Table S1; Taylor et al., 2012) to compare results of the detection and attribution analysis between those from GFDL-CM3 and all CMIP5 models. For consistency, only the CMIP5 models are selected for which ALL, AA, GHG, and NAT simulations are available and which have a spatial resolution finer than that of the observations.

Following Hsu et al. (2011) and Polson et al. (2014), we define the monsoon domain to encompass the grid boxes for which the observed annual precipitation range (difference between the May–September and November–March averages) exceeds 2 mm/day and more than 55% of the annual total precipitation occurs during May–September (see Figure S3). Our analysis is thus based on the climatological monsoon domain (i.e., the area is fixed throughout the period), which is a reasonable assumption as changes in monsoon precipitation associated with variations in the size or location of the region represent a minor contribution to the total precipitation change (Polson et al., 2014). Both observational data sets are interpolated to the same 2.5° × 2.5° grid before applying the above criteria. Grid boxes that have less than 70% land (based on a common land-sea mask) are excluded, and the South Asian region is limited to 90°E (e.g., Wang et al., 2001). For each region, this procedure gives one continuous monsoon area per observational data set, to which model data are masked before calculating regional mean time series in order to keep consistency with the respective observational coverage.

2.2. Linear Trends and Aerosol Emissions

The 1920–2005 period encompasses the peak of global anthropogenic aerosol emissions around 1980, driven by the changes in the Northern Hemisphere sulfate emissions. This global signal results from the combination of very different temporal evolutions of regional emissions, each with its different time of peak—some not yet peaked—and rate of increase/decrease following regional industrial development and air pollution regulations. Considering continental regions, North American emissions peaked around the 1970s and European emissions a decade later, while Asian emissions started to increase rapidly only from the 1950s (Figure S4) and are now the largest contributor to the global-aerosol loading. The simulated radiative forcing (e.g., Hansen et al., 2005) in the experiments with regional-aerosol emissions reflect these emission histories, both in the spatial patterns of long-term change (Figures S5a–S5d and S6) and in the time series over the emission regions (Figures S5e and S5f).

The spatial patterns of precipitation change are shown by computing the linear trend at each grid point. Trends are calculated over the entire 1920–2005 record as well as over two shorter subperiods, 1920–1975 and 1975–2005, separately. This allows us not only to characterize the long-term changes but also to distinguish between periods of increasing and decreasing North American and European emissions. Note that while Asian emissions increased both before and after 1975, their trend during 1975–2005 is twice as large as that over 1920–1975. The robustness of the ensemble mean trend at each grid point is measured by the number of ensemble members that agree on the sign of the changes. For each time period, the differences in the ensemble mean precipitation response between the experiments with regional-aerosol emissions only and the one with global-aerosol emissions are also shown, with a two-tailed Student's *t* test used to evaluate where the regional-aerosol ensembles are inconsistent with the AA ensemble at the 95% confidence level as a measure of the significance of the differences.

2.3. Detection and Attribution

The 1920–2005 time series of JJAS precipitation anomalies (with respect to the 1920–2005 climatology) are calculated for both observations and model simulations by averaging precipitation over each monsoon region and successively applying a 5-year running mean to reduce high-frequency variability. Total least squares regression (Allen & Stott, 2003) determines a scaling factor for the model ensemble mean time series, which defines the forced fingerprint, **F**, in observations

$$\mathbf{y} = (\mathbf{F} + \varepsilon_{\text{finger}})\beta + \varepsilon_{\text{noise}} \tag{1}$$

where **F** is a vector of length l, where l represents time, and **y** is a rank-l vector of the observed monsoon precipitation. β is the scaling factor corresponding to the magnitude of the forced fingerprint in the observations, $\varepsilon_{\text{noise}}$ is the noise associated with internal climate variability in the observations, and $\varepsilon_{\text{finger}}$ the internal variability associated with the finite ensemble size of the model simulations. Best estimates of just the forced component of the observations, $\tilde{\mathbf{y}}$, and of the model fingerprints, $\tilde{\mathbf{F}}$, are calculated using

$$\tilde{\mathbf{Z}} = \mathbf{Z} - \mathbf{Z}\tilde{\mathbf{v}}\tilde{\mathbf{v}}^T \tag{2}$$

where $\mathbf{Z} \equiv [\mathbf{F}, \mathbf{y}]$, $\tilde{\mathbf{Z}} \equiv [\tilde{\mathbf{F}}, \tilde{\mathbf{y}}]$, and $\tilde{\mathbf{v}}$ contains the eigenvector coefficients used to calculate β in equation (1).

Samples of climate noise, estimated from preindustrial control simulations from the CMIP5 models used, are then added to $\tilde{\mathbf{F}}$ and $\tilde{\mathbf{y}}$, and β is recalculated. The distribution of β gives thus the uncertainty on the scaling factor due to internal climate variability. Where $\beta > 0$ at the 5% significance level, the forced fingerprint is said to be detected. Because climate models tend to underestimate the observed temporal variability in JJAS total precipitation by a factor of 1.5–2 over the monsoon regions considered (Polson et al., 2014), we repeat the analysis, doubling the model variance when calculating the noise samples. Where a forcing is detected, we also test whether the variability of the residual, that is, the component of the observations not explained by the forcings, is not larger than expected from the 5–95% range of internal variability from the control samples as a consistency check.

The ALL fingerprint is a combination of the response to a number of different individual forcings that for the regions considered add approximately linearly (Figure S7). Our main one-signal analysis tests whether this combined forcing and which individual forcing can be detected when regressing them onto the observations one at a time. We also perform a two-signal analysis to see whether we can additionally separate the role of these individual forcings in driving the observed changes by simultaneously regressing two fingerprints onto the observations (see supporting information). For a detailed description of the implementation of the total least squares method see Polson et al. (2013).

3. Results

3.1. Spatial Patterns of Precipitation Change

During the whole period (1920–2005), observed precipitation exhibits a clear decrease across much of the West African and South Asian monsoon land regions (Figures 1a and 1b), which is also present in the GFDL-CM3 ALL ensemble and further extends to the nearby oceanic regions (Figure 1c). Comparison between the trends averaged over both monsoon regions (shown in blue and red in Figure S3a) for this period in the ALL ensemble (−0.043 mm/day/decade) with those in the single-forcing ensembles (Figures 1d–1f) indicates that this ALL drying pattern is dominated by the response to time-varying anthropogenic aerosols

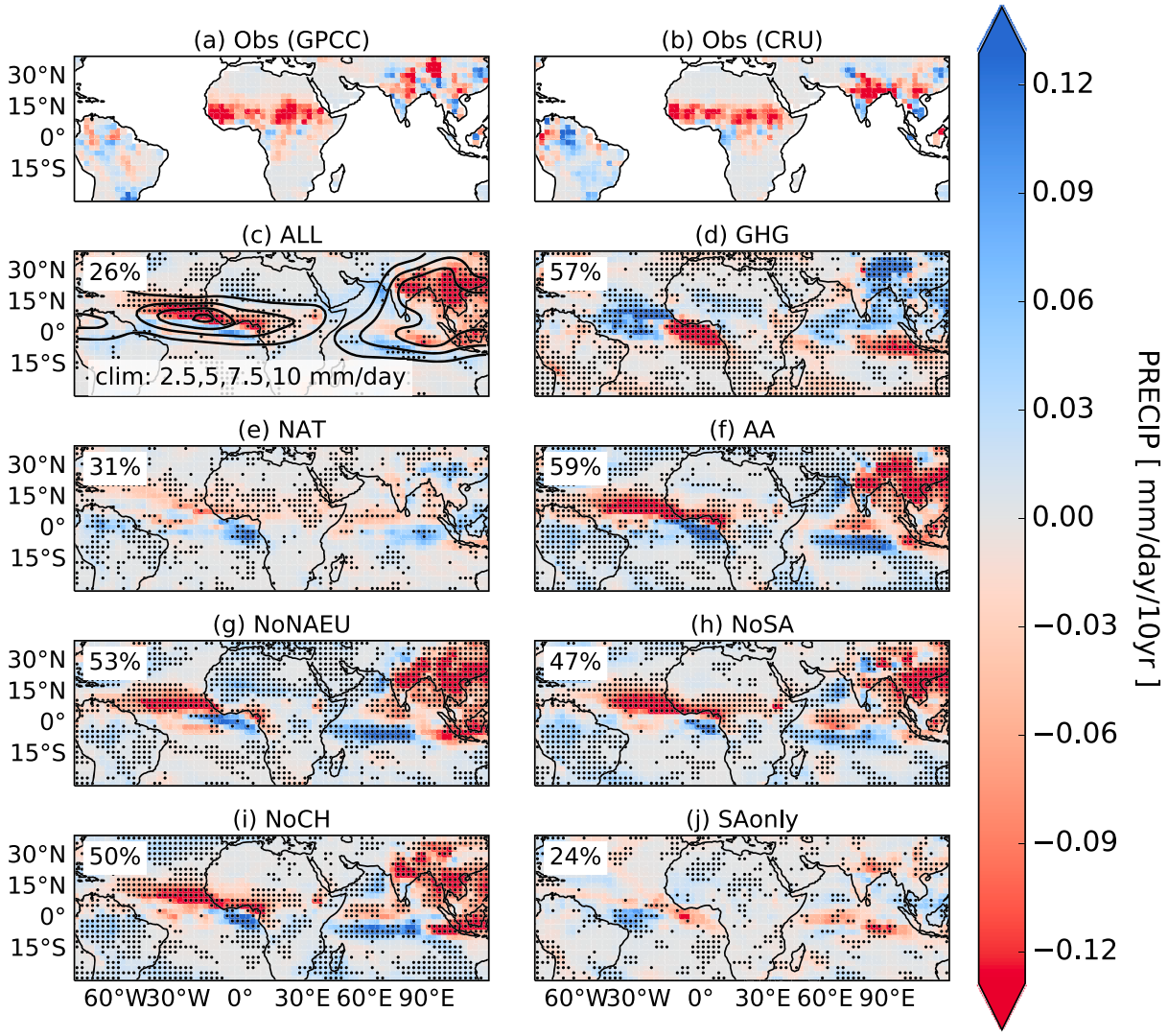

Figure 1. Observed and simulated summer (JJAS) precipitation linear trends (mm/day/decade) for 1920–2005. Shown are observed (a) GPCC and (b) CRU, and ensemble mean for (c) all external forcings (ALL), (d) greenhouse gas forcing (GHG), (e) natural forcing (NAT), and (f) global anthropogenic aerosol forcing (AA); global anthropogenic aerosol forcing with regional emissions set to preindustrial levels for (g) North America and Europe (NoNAEU), (h) South Asia (NoSA), (i) China (NoCH), and (j) all but South Asia (SAonly). Stippling shows where the respective ensemble agrees on the sign of the trend, and numbers in the top left corner give the fraction of stippled points within the displayed area. In (c), black contour lines (labels at the bottom) give the climatological summer (JJAS) precipitation from a 500-year preindustrial control simulation with the same model. See also Figure S10, which shows the same data only for the considered monsoon regions. JJAS = June–September. GPCC = Global Precipitation Climatology Centre; CRU = Climate Research Unit.

(-0.060 mm/day/decade for AA) and natural forcings (−0.015 mm/day/decade) rather than by GHGs, which cause a wettening instead (+0.032 mm/day/decade).

Across West Africa, the regional-aerosol experiments that include time-evolving North American and European emissions (NoSA and NoCH, Figures 1h, 1i), S10h, and S10i) produce a pattern of drying consistent with that of the global-aerosol ensemble (AA, Figures 1f and S10f). In the experiments that exclude these emissions, on the other hand, precipitation changes over the region are negligible and inconsistent (Figures 1g, 1j, S10g, and S10j). The ensemble mean AA trend averaged over the West African monsoon region (shown in blue in Figure S3a) amounts to −0.031 mm/day/decade. We interpret the difference in the ensemble mean trends of AA and NoNAEU (Figure 2b) as the trend induced by North American and European aerosol emissions alone and conclude that they cause a statistically significant trend of −0.035 mm/day/decade. This appears to be the largest contributor to the changes due to all but South Asian aerosols (−0.038 mm/day/decade for AA-SAonly, Figure 2e), and thus also the AA trend, while aerosols emitted from South Asia or China play a much smaller role (0.006 mm/day/decade for AA-NoSA, Figure 2c), and 0.005 mm/day/decade for AA-NoCH,

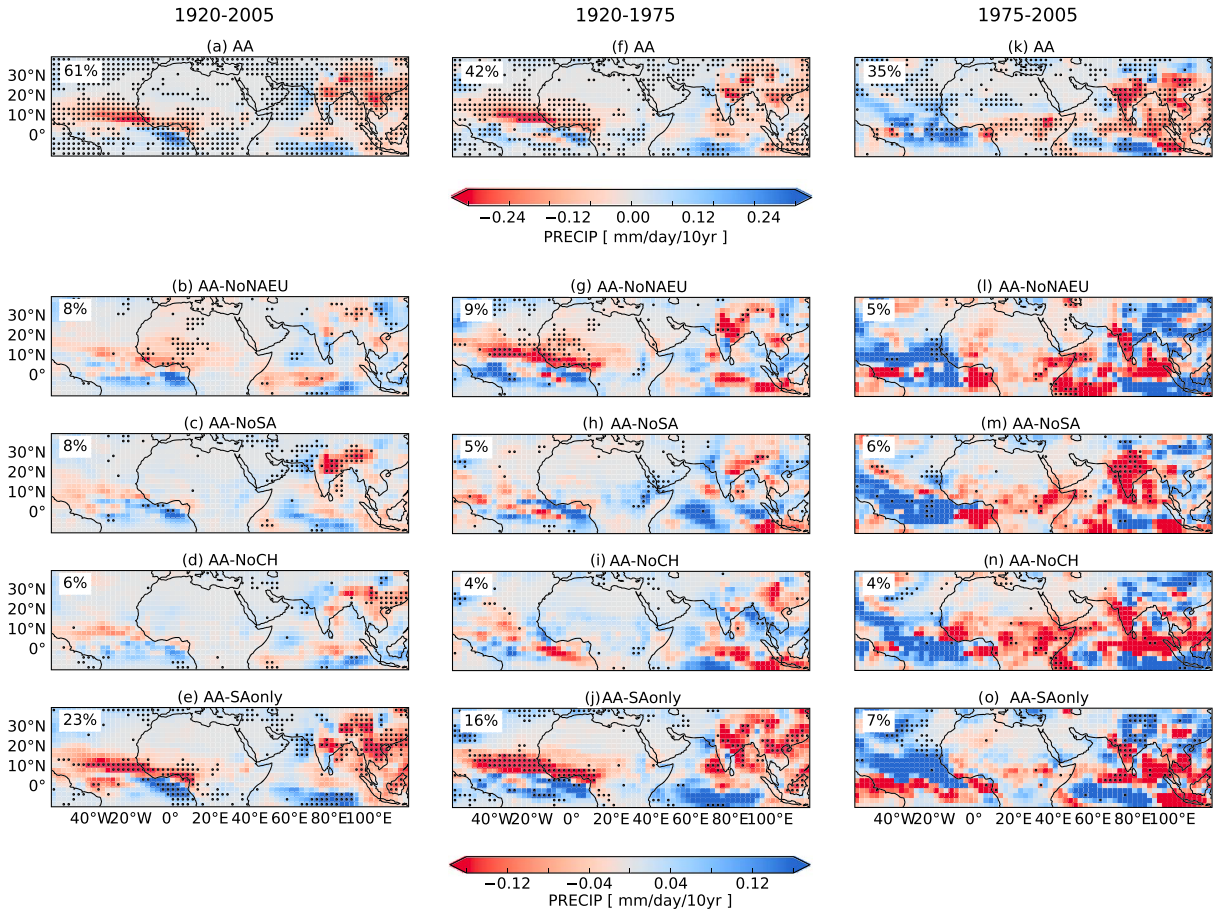

Figure 2. Simulated summer (JJAS) precipitation linear trends (mm/day/decade) in the global anthropogenic aerosol (AA) ensemble mean (first row) and the difference between the precipitation trends in the AA ensemble mean and the ensemble means of the regional anthropogenic aerosol simulations (mm/day/decade) for (a–e) 1920–2005, (f–j) 1920–1975, and (k–o) 1975–2005. The second row shows (b, g, l) AA-NoNAEU, indicating the impact of North American and European aerosols. The other rows show (c, h, m) AA-NoSA for South Asian aerosols; (d, i, n) AA-NoCH for Chinese aerosols; and (e, j, o) AA-SAonly for all but South Asian aerosols. Stippling in (a, f, k) shows where the AA ensemble agrees on the sign of the trend, and stippling in (b–e, g–j, l–o) shows where differences between the AA ensemble and regional-aerosol ensemble are statistically significant at the 95% confidence level using a *t* test. Numbers in the top left corner give the fraction of stippled points within the displayed area. JJAS = June–September.

Figure 2d). The long-term drying over West Africa related to non-Asian anthropogenic aerosol emissions is also dominant over changes related to other forcing agents (GHG, NAT), as illustrated by the differences in the trends between the ALL and the regional-aerosol ensembles (Figures S13a–S13e versus Figures 2a–2e).

The whole period (1920–2005) encompasses both the gradual increase in NAEU aerosols until 1975 (dominating the overall change) and the subsequent rapid decrease until 2005. Examining the two periods separately, Figures 2f–2o show that NAEU emissions were also the most influential driver of the 1920–1975 precipitation reduction in ALL and AA: The NoNAEU and SAonly simulations are statistically different at the 95% confidence level from the AA simulations over West Africa, while the NoSA and NoCH simulations are not (Figures 2g–2j); also Figures S8 and S11). The mean trend in the global-aerosol simulations over this time period (1920–1975) is 0.048 mm/day/decade over the West African monsoon region, which amounts to an overall change during 1920–1975 of nearly 10% of the climatological value of 3.4 mm/day (as calculated as the summer (JJAS) mean over the 500 years of a preindustrial control run). During the 1975–2005 period, an increase in precipitation is seen in observations in much of the West African monsoon region, especially in the North (Figures S9a, S9b, S12a, and S12b). The ALL, GHG, and AA ensemble means all show a similar pattern, indicating contributions from both GHG and ALL (Figures S9c, S9d, S9f, S12c, S12d, and S12f). However, there is still a decreasing trend in the AA ensemble mean of −0.017 mm/day/decade area-averaged across the region, and the sign of the trends are not consistent across simulations, suggesting that internal variability is too large compared to the forced signal during this period to clearly distinguish the influence of aerosol forcing.

Over South Asia, the largest drying trends during 1920–2005 in both the observations and the ALL and AA ensembles (Figures 1a–1c and 1f)) are over northern India. From Figures 2b–2e, we see that local emissions have a share in causing the aerosol-forced drying, as the NoSA and AA ensembles are statistically different. The combined influence of remote aerosols also seems to be important, as the SAonly and AA ensembles are also significantly different in northern India. Neither the NoNAEU nor the NoCH ensemble, however, show significant differences from AA in this region, which precludes the attribution of the AA trend to any specific aerosol source region. Across the South Asian monsoon region (shown in red in Figure S3a), global anthropogenic aerosols induce a precipitation decline of −0.089 mm/day/decade in the model, equivalent to an overall change during 1920–2005 exceeding 10% of the climatological value (7.4 mm/day). The differences between this and the ensemble means of the regional-aerosol simulations amount to −0.007 mm/day/decade for AA-NoNAEU, 0.003 mm/day/decade for AA-NoCH, and −0.064 mm/day/decade for AA-SAonly over this region (Figures 2b–2e). The value of −0.064 mm/day/decade for AA-NoSA indicates that local emissions are the largest single contributor to precipitation changes in the AA simulations during 1920–2005.

During the shorter periods, both observed and simulated precipitation trends over South Asia are generally more heterogeneous, and the simulated trends differ more from the observed ones (Figures S8, S9, S11 and S12). During 1920–1975, neither ALL nor AA are able to reproduce the observed wettening over western India (Figures S8 and S11). In the model, nonlocal emissions are again important to produce the AA trends (Figure 2j) and can in this case be related to NAEU emissions (Figure 2g), while the ensemble without South Asian emissions is not different from the AA ensemble (Figure 2h). During the second period (1975–2005), the spatial trend patterns of the two observational data sets differ more from each other than during the first half of the record, with CRU (Figure 2k) showing more drying in the northern and central parts of the South Asian monsoon region than GPCC (Figures S9a, S9b, S12a, S12b). The simulations are broadly consistent with either observational data set. During this period, both the increase of local South Asian emissions and the decrease of North American and European aerosols seem important for the changes in South Asian precipitation due to global anthropogenic aerosol forcing (Figures 2k–2o). The changes due to local aerosol emissions alone are also dominant over the changes due to GHG and NAT forcing (Figure S13).

3.2. Time Series of Precipitation Change

The above analysis of the spatial distribution of the precipitation trends across the West African and South Asian monsoon regions is here complemented by the study of the time series of area-averaged precipitation anomalies over the two regions. This yields additional information on the timing and time scale of these precipitation variations and provides support to the use of linear trends to estimate the changes.

Over West Africa, observed precipitation underwent a pronounced decrease from the 1960s to the mid-1980s, followed by a slight recovery until 2005 (Figure 3). Simulations that include time-varying anthropogenic aerosol emissions from North America and Europe (ALL, AA, NoSA, and NoCH) also show a decrease until the 1980s and a subsequent recovery, although the drying occurs here only gradually, in contrast to the observations. From 1945 to 1965 and in the early 1980s, the observations are only just consistent with or are outside the CMIP5 multimodel range (Figure 3a). This discrepancy may be due to errors in the observations or in the models' forced response, due to some aspect of internal variability not captured by the models including, for example, low-frequency variability in the ocean. We will account for this by increasing the control model variance in the detection and attribution analysis. Note also the steep decrease in observed precipitation followed by a rapid recovery in the first half of the 1980s, which is absent in the aerosol-only simulations, but visible to some extent in the simulations that include natural forcing (ALL and NAT; Figure 3a). It coincides with the El Chichón volcanic eruption in 1982, which is consistent with other studies that find drying in monsoon regions after volcanic eruptions (e.g., Iles et al., 2013).

South Asian monsoon precipitation shows a decrease during the second half of the twentieth century on top of large background decadal variability (Figure 4). Only the simulations with time-varying emissions from South Asia closely resemble this observed decrease in precipitation (ALL, AA, NoNAEU, NoCH, and SAonly). Note the spread between the two observational data sets from the 1980s onward, with noticeable differences in the 1990s. This is likely due to differences in station coverage as data availability tends to reduce toward the end of the twentieth century (Schneider, Becker, et al., 2014).

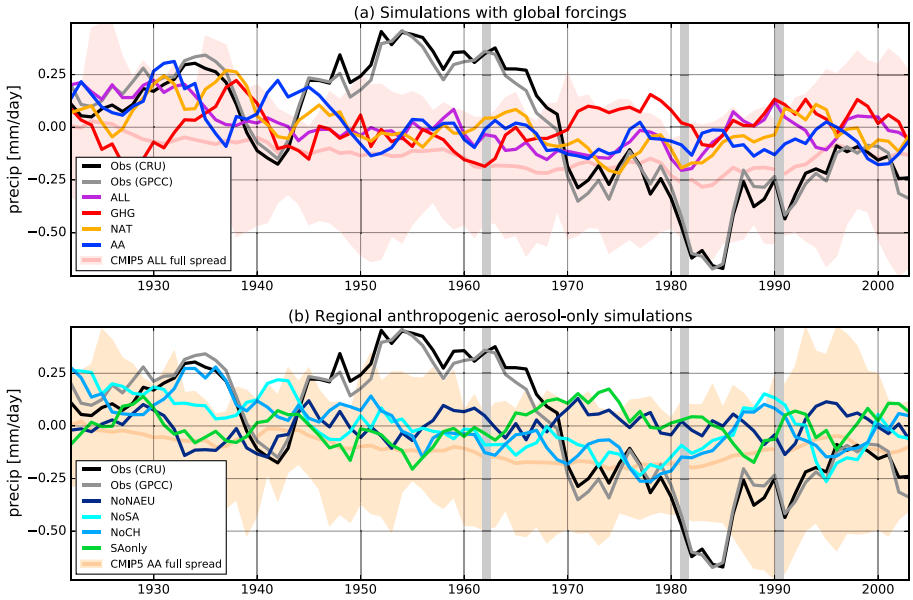

Figure 3. West African summer (JJAS) monsoon precipitation anomalies (mm/day) with respect to the 1920–2005 climatology for observations [CRU (black) and GPCC (gray)] and ensemble mean anomalies for GFDL-CM3 simulations with (a) global forcings and (b) regional anthropogenic aerosol forcings (ensemble abbreviations as in Figure 1). The 5-year running mean is shown for all time series; note that the simulated ones are ensemble means and have thus reduced variability compared to (single-realization) observations. Pink and orange shading, respectively, show the model spread for all (a) CMIP5 ALL and (b) CMIP5 AA historical simulations. All model data are masked using the monsoon region derived from the CRU data. Silver vertical lines show large volcanic eruptions. Figure S14 shows the same time series multiplied by the respective best guess scaling factors from the one-signal detection and attribution analysis. JJAS = June–September. GPCC = Global Precipitation Climatology Centre; CRU = Climate Research Unit.

3.3. Detection and Attribution

A detection and attribution analysis (see section 2.3) can link changes in monsoon precipitation and individual forcing agents in a statistically rigorous manner, explicitly taking into account climate variability, which is large for precipitation. Using this approach, Polson et al. (2014) showed that anthropogenic aerosols are the dominant external factor influencing the observed changes in Northern Hemisphere summer monsoon precipitation during the second half of the twentieth century: Using CMIP5 multimodel mean (MMM) fingerprints to explain the observed time series of precipitation during 1951–2005 averaged over the whole Northern Hemisphere monsoon domain (thus including the South American, West Africa, South Asian, and East Asian monsoon regions), the authors detected the response to global-aerosol forcing in four different observational data sets, while no other external forcing was detected, and the observed changes could not be explained by internal climate variability alone either. However, the detected change was significantly larger than simulated. Motivated by these results, we test here whether global-aerosol forcing also dominates the observed changes during 1920–2005 in the West African and South Asian monsoon regions separately, and whether we can distinguish the importance of the different source regions for AA by detecting the fingerprints from the different regional anthropogenic aerosol simulations in the observations. This analysis considers the time series of precipitation change rather than just the linear trend as done previously, which is especially important given the different temporal evolutions of aerosol emissions from different source regions.

For West Africa, Figure 5a shows that the external forcings (ALL) both from the CMIP5 MMM and GFDL-CM3 are detected in both observational data sets (scaling factors > 0). The observed changes are underestimated in the models, since the forced response must be scaled up (i.e., the lower bound of the scaling factor range for ALL exceeds 1). This is consistent with the observations showing stronger trends than the all-forcing CMIP5 simulations in Figure 3a. This result is robust to doubling the model internal variability, which means that the forced response is detected even if the models turned out to underestimate observed variability by a factor of 2. When the variability is doubled, the residual consistency check is passed in all cases. The global-aerosol (AA) fingerprints are also detected, while the GHG ones are not (Figure S16a), indicating the importance of aerosols rather than GHG. When using the GFDL model, NAT is also detected, while this is not the case for

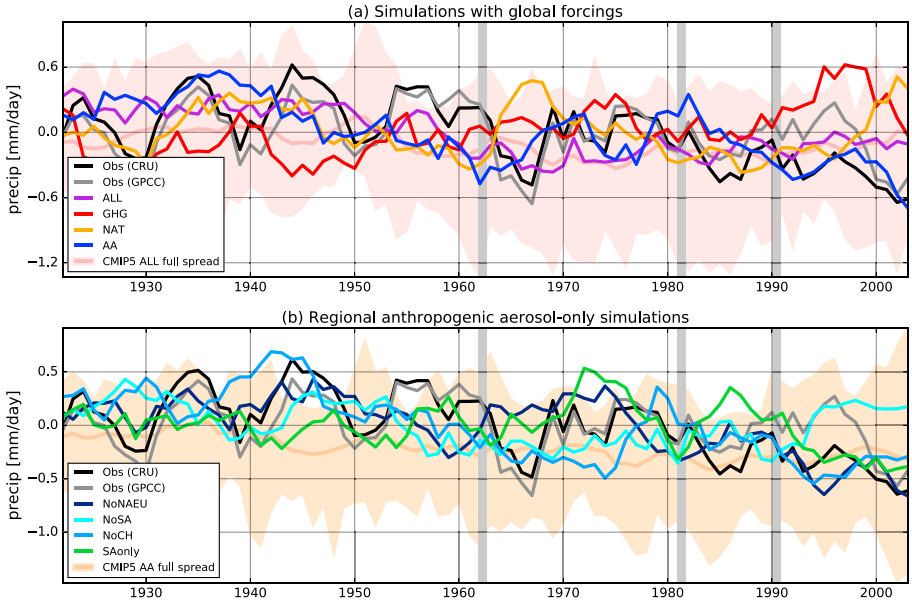

Figure 4. As in Figure 3 but for South Asian monsoon precipitation anomalies (mm/day). Figure S15 shows the same time series multiplied by the respective best guess scaling factors from the one-signal detection and attribution analysis.

the CMIP5 MMM, possibly due to a stronger response to volcanic aerosols in the GFDL model compared to the other models. A two-signal analysis, performed to disentangle the role of the individual global forcings, for example, NAT versus AA, is inconclusive (Figures S17–S19), indicating that the forcings are likely too weak or the responses too similar to be detected simultaneously given internal variability. Our results nevertheless suggest that aerosols play a key role for the changes in West African monsoon precipitation. Out of the aerosol source regions, North America and Europe are found to be essential to drive these precipitation changes. That is, when emissions from these regions are included in the model fingerprints, they are detected (NoSA, NoCH, ALL, and AA), otherwise they are not (SAonly and NoNAEU).

For South Asia (Figure 5b), a forced response in summer monsoon precipitation is only detected if CRU observations are used (i.e., not the GPCC data set). The difference in the detection and attribution results between these observational data sets is likely related to the previously discussed discrepancies in the time series in the 1990s, and we discuss here the results for CRU. When using the CMIP5 MMM, both the NAT and the AA fingerprints are detected, but not ALL, which is likely explained by the GHG forcing counteracting the aerosol forcing in ALL. When using GFDL-CM3, the fingerprint of the combined forcings (ALL) is detected—while GHGs and aerosols also counteract each other in this model, the ALL signal from GFDL-CM3 is more influenced by anthropogenic aerosols than the ALL signal from the CMIP5 MMM, likely because GFDL-CM3 has a stronger indirect aerosol forcing than most other models (Zelinka et al., 2014), which are included in the CMIP5 MMM. When doubling the model internal variability, none of the signals is detected for the CMIP5 models. When using GFDL-CM3, we detect the fingerprints of all external forcings (ALL) and of global aerosols (AA), but neither those of NAT nor GHG (Figures 5b and S16b), which shows the importance of anthropogenic aerosols as simulated with GFDL-CM3 also for South Asian monsoon precipitation. The residual consistency check is passed in all cases. The scaling factors are here consistent with 1; that is, the combination of the forcing strength and the magnitude of the model response reproduces the magnitude of the observed changes. In contrast to West Africa, local aerosol emissions seem to be the most important factor driving the observed changes in South Asia: Aerosol forcing is only detected when historical variations of South Asian aerosol emissions are included (ALL, AA, NoNAEU, NoCH, and SAonly). In fact, only South Asian emissions (SAonly) are required for the aerosol forcing to be detected, at least for the best estimate of model internal variability. Conversely, aerosol forcing is not detected when emissions from South Asia are kept at preindustrial levels (NoSA). These results are confirmed by a two-signal analysis, where we can detect the response to global-aerosol forcing versus all other forcings together (Figure S18) as well as the response of the simulations which include local aerosols for CRU in three out of four cases (Figure S19).

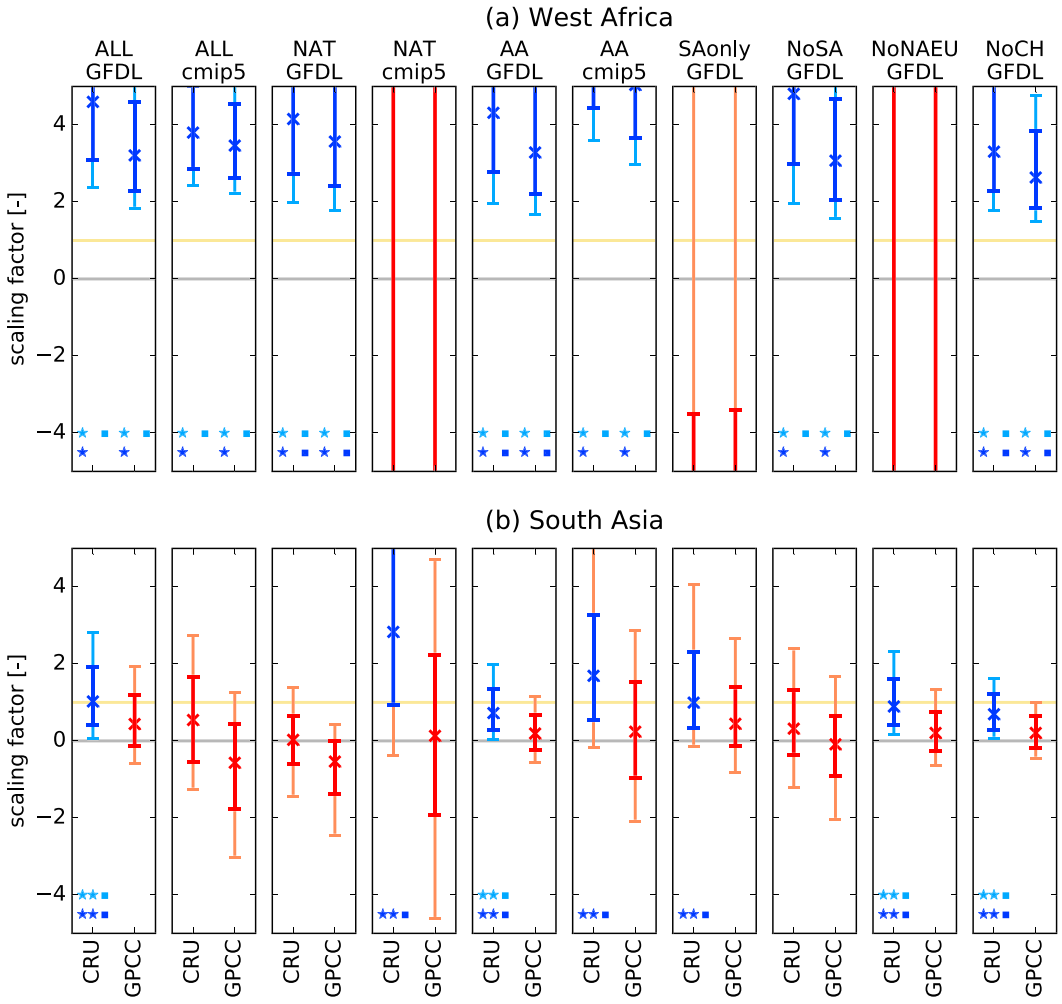

Figure 5. Detection and attribution of observed changes in (a) West Africa and (b) South Asia summer (JJAS) monsoon precipitation from the one-signal analysis. Scaling factors for global forcings from GFDL-CM3 (GFDL) and the CMIP5 MMM (cmip5), and regional anthropogenic aerosol-only forcing from GFDL-CM3 (ensemble abbreviations as in Figure 1); results for GHG forcing in Figure S16. Results are shown for two observational data sets, CRU (left) and GPCC (right). Crosses show the best guess scaling factor for the ensemble mean, thick lines are the 90% confidence interval based on the raw variance of the model control samples, and thin lines are the 90% confidence intervals when the variance has been doubled. Lines are blue when detected, red when not. The detection of a signal is further highlighted by one star (*), and two stars of the same color next to each other (**) show where the forcing is additionally consistent with a scaling factor of 1. A filled square indicates where the variance of the residual is not larger than internal variability at the 95% confidence interval based on the raw variance of the model control samples. Light blue stars and squares as well as light blue and light red lines refer to the calculation with doubled variance. JJAS = June–September; GFDL = Geophysical Fluid Dynamics Laboratory; CMIP5 Coupled Model Intercomparison Project 5; MMM = multimodel mean; CRU = Climate Research Unit; GPCC = Global Precipitation Climatology Centre.

4. Pathways of Aerosol Impact

4.1. West Africa

The annual cycle of the West African monsoon precipitation is linked to the migration of the ITCZ, although the two phenomena have also distinct features (Nicholson, 2013). Yet this classical view provides a useful framework to interpret monsoon changes in the context of large-scale circulation variations. The AA spatial pattern of 1920–2005 precipitation trends across the Atlantic show that global aerosols caused a decrease in precipitation at the climatological northern flank of the ITCZ and an increase at its southern flank, consistent with a southward shift of the Atlantic ITCZ (Figure 1f). The aerosol signature clearly dominates the ALL pattern. Furthermore, it is also present in all regional-aerosol experiments but for SAonly. For West Africa, this means a decrease in precipitation over the coastal land areas and an increase in precipitation over the ocean to the south, thus outside the summer monsoon region.

To track the meridional displacement of precipitation across the Atlantic basin throughout the twentieth century, the latitude of maximum precipitation longitudinally averaged over 75°W to 50°E (see Figure S3; Philander et al., 1996; Schneider, Bischoff, et al., 2014) is shown in Figure 6. The southward displacement of precipitation is notable in simulations with aerosol emissions from North America and Europe (Figures 6a, 6d, 6f, 6g, and 6i), with the fastest changes between the 1940s and 1960s, consistent with those in emissions (Figure S4). In simulations without emissions from these regions, in contrast, the shift occurs only at the end of the twentieth century (Figures 6e and 6h). Theoretical considerations suggest interhemispheric temperature differences to drive the shift in the ITCZ; for aerosols, this is due to the preferential cooling of the Northern Hemisphere (Hwang et al., 2013; Rotstayn et al., 2015). The spatial patterns of long-term sea surface temperature (SST) change illustrate the hemispheric differences for the differently forced experiments (Figure S20). The time series of the interhemispheric temperature difference agree well with the latitudinal position of the ITCZ, with statistically significant correlations of over 0.8 for all simulations but ALL and SAonly on multidecadal time scales (Figures 6b–6g), and over 0.7 for ALL (Figure 6a). The much smaller correlation for SAonly (Figure 6h) is not surprising given its weak forcing. Observations for land-only precipitation also show a similar tendency for a southward shift from the 1960s, while the satellite observations show a tendency for a northward shift in the latitude of maximum precipitation from the mid-1980s, similar to the models. These precipitation shifts are even clearer in the observations when the South American longitudes are excluded, and the correlations are similar if only SSTs are used to calculate the interhemispheric temperature gradient (not shown). The model simulations show that the northward shift in recent decades due to decreasing NAEU emissions (Figure 6f is weakened by the southward shift induced by non-NAEU emissions; Figure 6h). Note that also within the non-aerosol simulations (GHG, Figure 6b and especially NAT, Figure 6c), interhemispheric temperature difference and meridional ITCZ position correlate, consistent with a causal relationship between the two. The long-term decrease until the 1980s seen in ALL and the observational datasets, however, is inconsistent with the increase in GHG, and much more clear in the aerosol simulations than in NAT. The classic interpretation of the West African monsoon precipitation as part of the ITCZ is thus functional here and the shift of the ITCZ, consistent with aerosol-induced changes in the interhemispheric temperature difference, explains part of the changes in West African monsoon precipitation.

The statistically significant difference in West African summer monsoon precipitation between the simulations including all aerosols and those excluding aerosols from anywhere but South Asia could point not only to the impact of aerosols from the major Northern Hemisphere emission regions but also to a role of local (West African) emissions (Figure S21), as found, for instance, in recent trends for black carbon in winter (Huang et al., 2009). Simulated clear-sky shortwave downward radiation and surface temperature in the West African monsoon region diverge indeed depending on whether local aerosol emissions are included (NoNAEU, NoSA, and NoCH) or not (SAonly; Figures 7c and 7e): With local emissions, the clear-sky radiation reaching the surface decreases throughout the twentieth century concurrent with an increase in local aerosol emissions (Figure 7a). All-sky downward radiation (Figure 7d), which, in contrast to clear-sky radiation, takes into account cloud cover and thus also reflects circulation changes, does not show this dependency on local emissions, and neither does precipitation (Figure 7f). Instead, precipitation depends on whether North American and European emissions are included (NoSA and NoCH) or not (NoNAEU and SAonly), which is consistent with the signals detected in the previous section. While local aerosol emissions may thus still have some impact on precipitation, the combined effect of remote aerosols, mainly from North America and Europe, dominates the changes in West African summer monsoon precipitation. Since clear-sky radiation over West Africa, indicative of aerosol-radiation interactions, does furthermore not change whether NAEU emissions are included (NoSA and NoCH) or not (NoNAEU), aerosols transported to West Africa, if any, are of minor importance compared to the cloud changes associated with large-scale circulation patterns from remote aerosol cooling.

4.2. South Asia

For South Asia, the monsoon precipitation is more independent from the ITCZ, which is in this region located over the Indian Ocean, that is, farther south than the considered monsoon region. The decreased precipitation detected for all simulations including South Asian aerosols (i.e., all but NAT, NoSA, and GHG in Figure 5b) is related to a weakened monsoon circulation, as visible for instance in counterclimatological 1920–2005 trends of 850 hPa wind (Figures 8a and S22). This anomalous easterly flow over India and along the coasts of the Arabian peninsula and East Africa is associated with the aerosol-induced cooling of the land with respect to the ocean and a related increase in surface pressure over land (Figures 8f and 8k). Nonlocal aerosols are most important for these long-term trends (Figures 8b–8e, 8g–8j, and 8l–8o), which is consistent with the

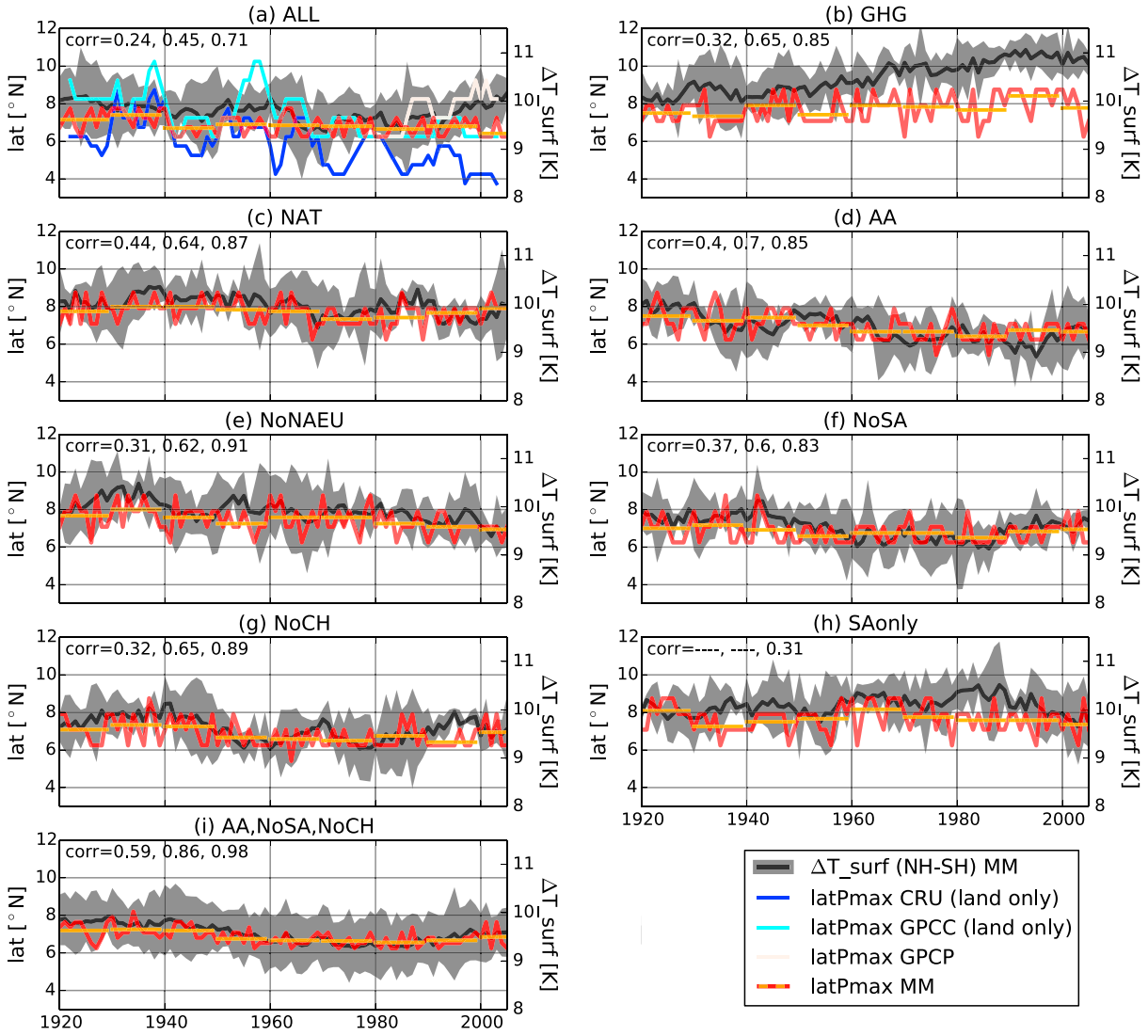

Figure 6. Latitude of maximum zonal mean precipitation (latPmax) over the Atlantic sector (75°W–50°E; shown by the yellow box in Figure S3; left axis, in color) as well as interhemispheric temperature gradient (ΔT_surf, land and ocean) for the same longitudes (right axis, black). The ensemble mean time series of latPmax [annual (JJAS) = red lines; decadal means = yellow lines] and ΔT_surf [annual (JJAS) = black; 95% ensemble range = gray shading] are shown for the simulations with (a–d) global forcings and (e–h) regional-aerosol forcings (ensemble abbreviations as in Figure 1); (i) shows the average across the nine simulations with evolving NAEU emissions. Numbers at the top of each panel give the correlation coefficient between ΔT_surf and latPmax for annual time series (as shown), the 5-year running mean, and the 11-7-year running mean, where statistically significant (pval < 0.05). In (a), latPmax is also shown for the GPCP observations (creme-white), CRU observations for land only (blue), and GPCC observations for land only (cyan), all smoothed with a 5-year running mean. NAEU = North America and Europe; CRU = Climate Research Unit; GPCP = Global Precipitation Climatology Project; GPCC = Global Precipitation Climatology Centre.

findings for precipitation (Figures 2b–2e; note the increased importance of local aerosols in the last decades of the twentieth century (Figure 2k). While the aerosols dominate the ALL response, GHGs act conversely to strengthen the circulation (Figures S22–S24).

More evidence for this weakening of the circulation, and the aerosols' role in this, is seen in the time series of regional mean sea level pressure, zonal wind, and land-sea temperature contrast, shown in Figure 9 along with their respective correlation coefficients on short (annual time series) and longer time scales (time series smoothed by 11- and 7-year running means applied consecutively): variations in zonal wind speed over India and the Arabian Sea, on the one hand, and precipitation, on the other hand, closely resemble each other on longer time scales [correlations > 0.85 for the latter for all simulations but NAT (Figure 9c) and SAonly (Figure 9f), second blue numbers], and sea level pressure over South Asian land and adjacent areas to the North varies in opposite phase with precipitation (Figure 9, orange numbers). All simulations that include not

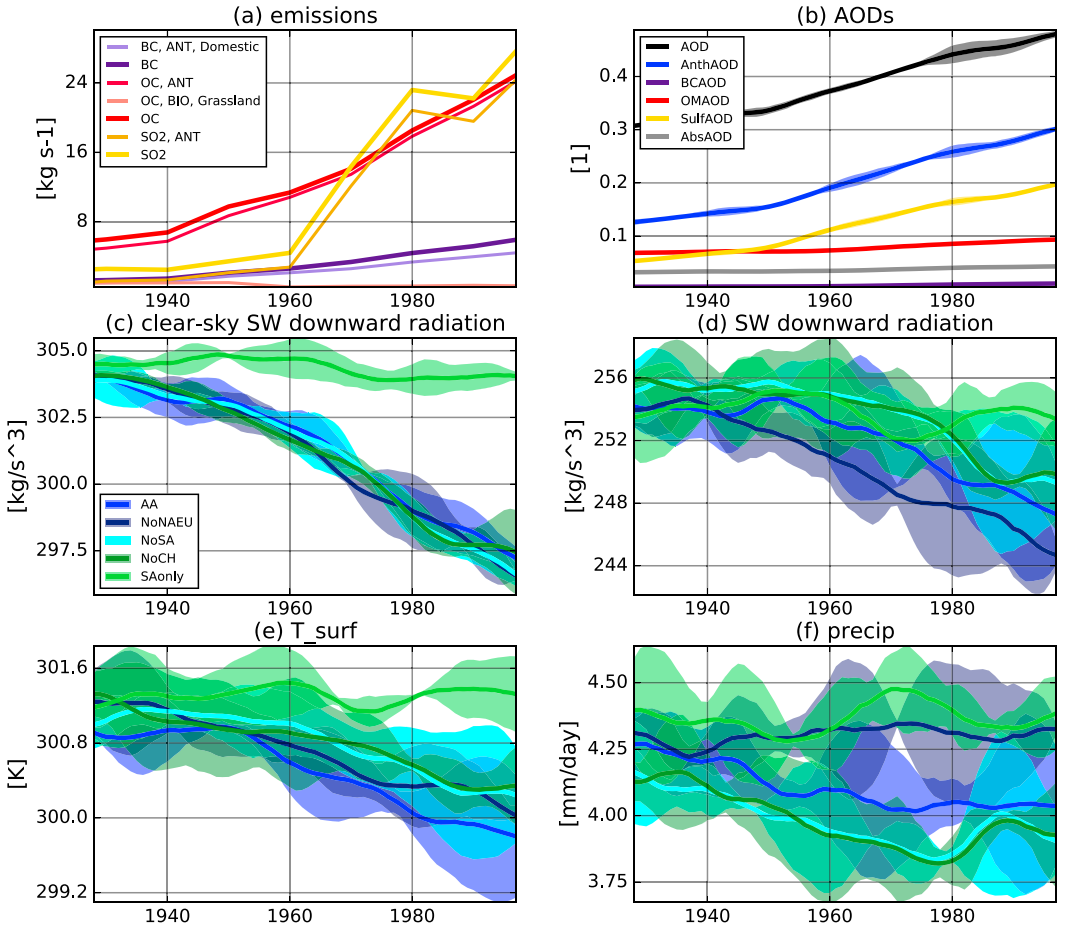

Figure 7. West African summer (JJAS) (a) total aerosol emissions from Lamarque et al. (2010) as used in the simulations and (b) aerosol optical depth (AOD) from the aerosol-only (AA) simulations' ensemble mean as well as (c) clear-sky shortwave downward radiation, (d) all-sky shortwave downward radiation, (e) surface temperature, and (f) precipitation as simulated with global anthropogenic aerosol only forcing (AA) as well as regional-aerosol simulations (ensemble abbreviations as in Figure 1). Shown are 11-7-year running means along with their respective 95% range of the individual simulations (shading). In (a), total emissions of black carbon (BC), organic carbon (OC), and sulfur dioxide (SO_2) are shown along with the contributions from grassland fire emissions (BIO, Grassland) for all species and combined energy, transportation, domestic, industrial, waste treatment, and agricultural waste burning sector emissions (ANT) for OC and SO_2. In (b), total AOD (black) and absorbing AOD (gray) also include other aerosol species, for instance, dust aerosols, the emission sources of which are prescribed climatologically in the model. AODs due to sulfate aerosols (yellow), black carbon (purple), and organic matter (red) and their sum, the anthropogenic contribution to AOD (blue), are also shown. Area means are taken over (a) the land area within 4°N–17.5°N, 20°W–42.5°E, and (b-f) the West African monsoon region (shown in blue in Figure S3a). JJAS = June–September.

only South Asian aerosols (Figures 9a and 9d–9g) show this weakening of the circulation until about 1970, while the inclusion of South Asian aerosols (Figure 9h) is necessary to continue this trend in the later decades.

The temperature contrasts between South Asian land and ocean (Figure 9) as well as between Northern and Southern Hemispheres (not shown) are crucial drivers of the monsoon and exhibit the same long-term trends as precipitation (second purple numbers in Figure 9). Precipitation in the ALL simulations, however, is more clearly dominated by the aerosol forcing than it is in the case for the temperature gradients (Figure S25), which might reflect other means of aerosol impact contributing to the weakening of the monsoon circulation.

When forced with observed SSTs, the model simulates a pattern of precipitation change even closer to the observed one and, indeed, more so than some reanalysis products (Figures S26m and S26n; Compo et al., 2011), which improves our trust in the reliability of the model-based findings. While the observed SSTs include the slow component of the response to external forcings, the fast component of the response must also be included in order to recover the full signal (Figures S26o and S26p). The consistency between the circulation

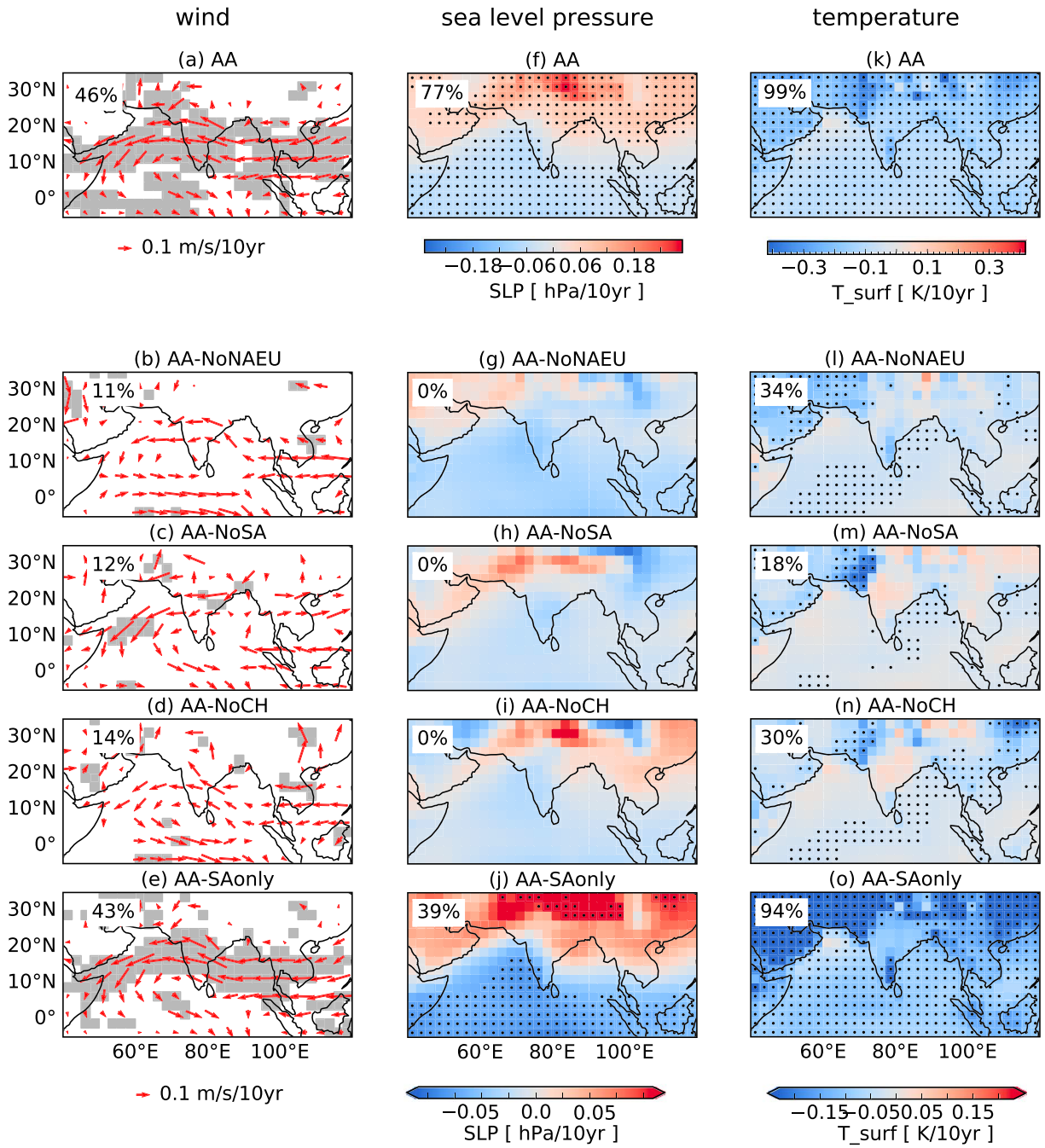

Figure 8. Simulated 1920–2005 summer (JJAS) ensemble mean linear trends in the global anthropogenic aerosol simulations (AA) (first row) and differences between these and the ensemble mean trends of the regional anthropogenic aerosol simulations (other rows) for wind speed at 850 hPa (left), sea level pressure (SLP, middle), and surface temperature (*T*_surf, right). These differences indicate the impact of aerosols from (b, g, l) North American and European, (c, h, m) South Asian, (d,i,n) Chinese, and (e, j, o) all but South Asian sources. In the first row, gray shading (a) or stippling (f, k) shows where the AA ensemble agrees on the sign of the trends in (a) zonal, meridional, and total wind speed, (f) SLP, and (k) *T*_surf. In the other rows, shading (b–e) or stippling (g–j, l–o) shows where differences between AA ensemble and regional-aerosol ensemble are significant at the 95% confidence level using a *t* test. Numbers in the top left corner give the fraction of stippled points within the displayed area. JJAS = June–September.

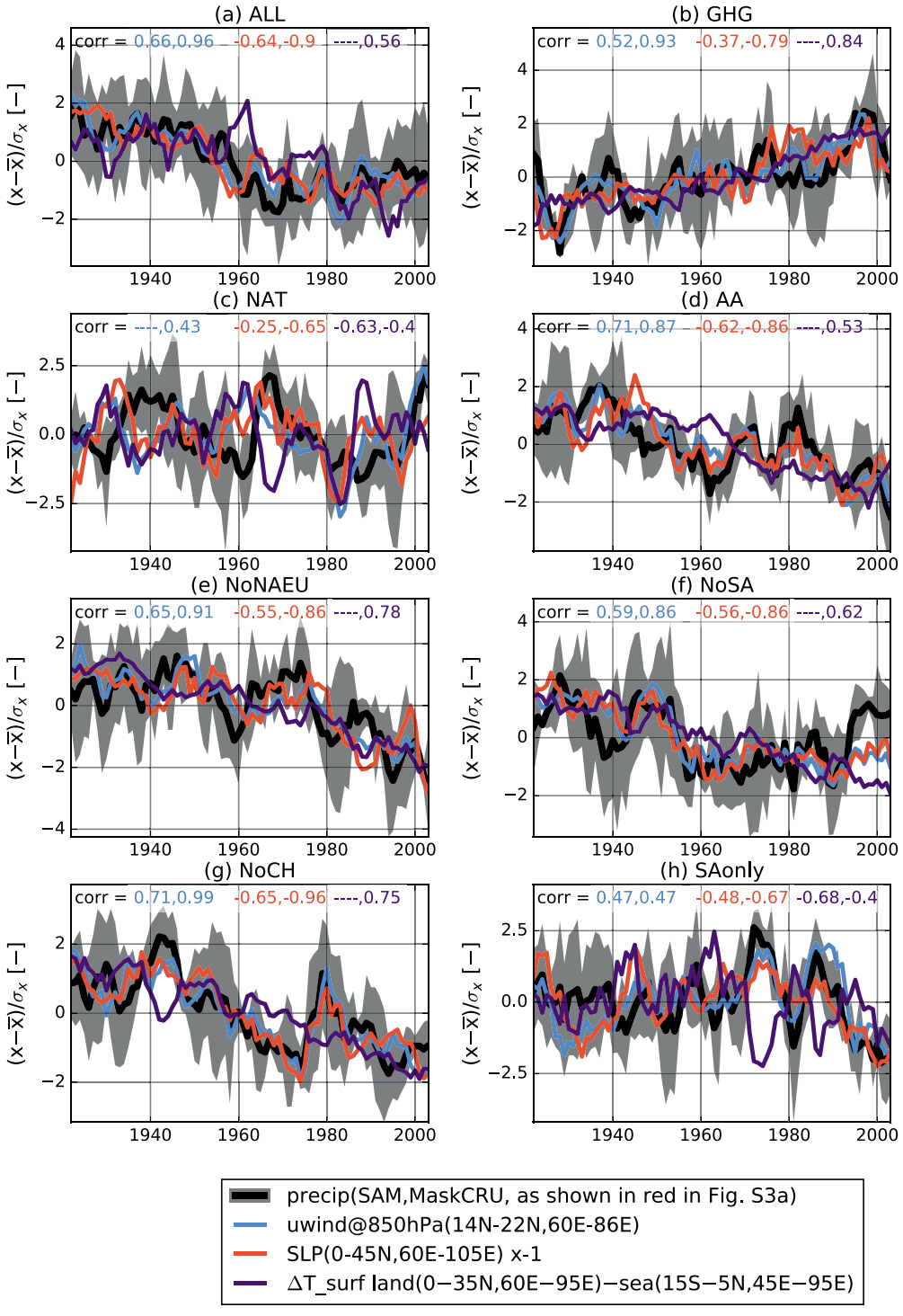

Figure 9. Standardized South Asian summer (JJAS) monsoon precipitation anomalies (black), zonal wind speed over India and the Arabian Sea (light blue), sea level pressure over a northerly extended South Asian land region (orange), and surface temperature difference between South Asian land and northern Indian ocean temperatures (purple) for 1920–2005 for the ensemble mean of (a-d) global forcings and (e–h) regional-aerosol forcings. Shown are the 5-year running means along with their respective 95% range of the individual simulations (shading). Numbers at the top of each panel give the correlation coefficient between precipitation and each of the other variables for the nonstandardized annual time series (first number), and the 11-7-year running mean (second number), where statistically significant (pval < 0.05). The correlation between near-surface (2 m) temperature (not shown) and precipitation on long time scales amounts to 0.83. JJAS = June–September.

changes over the South Asian monsoon region between the fully coupled AA and ALL experiments, on the one hand (Figures S22–S24), and when forced with observed SSTs, on the other hand (Figures S26a–S26l), shows furthermore that the contribution of long-term ocean variability as well as ocean-atmosphere coupling is of secondary importance to the aerosol-related changes shown above.

5. Discussion and Conclusions

A number of studies have shown that precipitation in monsoon regions across the Northern Hemisphere underwent large changes during the twentieth century. Anthropogenic aerosols have been shown to have influenced the observed changes above internal variability and dominate over GHG forcing which on its own would have led to an increase in precipitation (Polson et al., 2014). By extending the analysis period back to the 1920s, we have been able to show that in two individual monsoon regions, West Africa and South Asia, anthropogenic aerosols have driven observed changes in precipitation and that the source region of the aerosol emissions is an important factor in the detectability of anthropogenic aerosol forcing. However, the models' significant underestimate of the magnitude of the observed changes remains a concern.

For West Africa, remote aerosols from North America and Europe need to be included in order to detect the anthropogenic signal in observed monsoon precipitation. The decrease in precipitation seen from the 1950s to 1980s and the subsequent recovery agrees with the evolution of total global emissions, of which these regions are the largest contributor (Figure S4; see also Polson et al., 2014). This is consistent with the changes in West African precipitation being partly related to shifts in the ITCZ due to the interhemispheric temperature differences caused by the aerosol preferential cooling of the Northern Hemisphere (Hwang et al., 2013; Rotstayn et al., 2015). Nevertheless, the models underestimate the magnitude of the observed changes, and the strong drying seen during the middle of century is not captured by GFDL-CM3. This results in large best estimate scaling factors, which raise questions whether the models correctly capture the monsoon response to aerosol forcing (see Figure S14). Other studies have shown that CMIP5 models tend to underestimate the observed multidecadal trends in the Sahel (Biasutti, 2013), which may be due to weaker forcing or missing physical processes in the models, for example, indirect aerosol effects (Booth et al., 2012), changes in dust aerosols (Ji et al., 2016), or land surface feedbacks (Kucharski et al., 2013), or due to internal variability, such as from SSTs (Ting et al., 2009). The CMIP5 models' ability to simulate the connection between North Atlantic SSTs and Sahel precipitation varies (Martin et al., 2014), but this does not seem to influence the detectability of aerosol response, since ALL and AA are detected both for GFDL-CM3 and the CMIP5 ensemble. The West African monsoon region identified in this study has some overlap with the Sahel region considered by Dong and Sutton (2015), who found GHGs and, to a lesser extent, aerosols, not SST trends, necessary to explain the recovery of Sahel precipitation with the HadGEM model. Volcanic eruptions in the 20th century may also be important drivers of variability at shorter time scales, and aerosols from volcanic eruptions have also been shown to cause the shift in the ITCZ away from the hemisphere where the aerosols cooling is larger (e.g., Iles & Hegerl, 2015).

In contrast, in South Asia, where changes in local aerosol emissions are larger than for West Africa, local emissions are essential in order to explain observed changes in monsoon precipitation. This is consistent with increasing emissions from South Asia during the later part of the twentieth century and with studies that find the indirect aerosol effect acting locally plays an important role in the decline in precipitation in this region (Guo et al., 2015). While our results suggest that anthropogenic aerosol forcing has played a role in driving the observed drying, this does not preclude an additional role by decadal variability, for example, the Pacific Decadal Oscillation (Salzmann & Cherian, 2015), which, however, might also have been influenced by an aerosol-induced change in the Walker circulation via modulation of the trade wind strength (Dong, Zhou, et al., 2014; Takahashi & Watanabe, 2016).

For both monsoon systems, the failure to detect anthropogenic aerosol forcing from other source regions should not be interpreted as these aerosol emissions having no influence, but rather that they are not detectable above the internal variability of precipitation during the period 1920–2005. Modeling studies of the Asian monsoon (Cowan & Cai, 2011; Dong et al., 2015), and the analysis of the spatial trends patterns here, suggest that both local and non-Asian aerosols contribute to the weakening of the monsoon, while studies of West Africa suggest that aerosol emissions from Asia also play a role in this regional reduction in monsoon precipitation (Dong, Sutton, 2014). This analysis provides more rigorous support to the results of the modeling study of Bollasina et al. (2014) who suggested a predominance of local aerosols in driving seasonal mean

precipitation changes over South Asia, and, in particular, the widespread monsoon decrease over central India. Note, they also found that nonlocal aerosols were of greater importance for early summer precipitation changes associated with an advanced monsoon onset, which, in terms of seasonal mean anomalies, results in the positive precipitation anomaly over northwestern India.

Uniquely, we have been able to show that the influence of local anthropogenic aerosols in South Asia, and of North American and European emissions in West Africa, is not only recognizable in the model simulations but also detectable in long-term observations of precipitation. While our results rely on simulations with the GFDL-CM3 model, we believe them to be robust, since key features of the aerosol response are also in the CMIP5 MMM. However, reproduction of the study with a larger ensemble and other models would be important to provide further support to the robustness of the results. The detection of aerosol influence on past monsoon precipitation changes highlights the possible role of the decline in anthropogenic aerosol emissions expected in the near future (Vuuren et al., 2011), with the interplay of aerosols from different source regions likely gaining importance due to more heterogeneous global emission patterns.

Acknowledgments
The authors acknowledge the use of precipitation data of the Global Precipitation Climatology Centre, and the Climatic Research Unit. We thank the World Climate Research Programme's Working Group on Coupled Modelling, the climate modeling groups (Table S1), the U.S. Department of Energy's Program for Climate Model Diagnosis and Intercomparison, and the Global Organization for Earth System Science Portals and thank the reviewers for their useful comments. This work was supported by the European Research Council (ERC) funded project (EC-320691) TITAN. G. Hegerl is funded by National Centre for Atmospheric Science (NCAS) and the Wolfson Foundation and the Royal Society as Royal Society Wolfson Research Merit Award holder (WM130060). The observational data sets as well as CMIP5 data used in this study are publicly available and properly cited and referred to in the reference list, and the precipitation data from the GFDL-CM3 experiments are available at https://doi.org/10.6084/m9.figshare.5777907. Other fields from those experiments are available upon request from the third author (massimo.bollasina@ed.ac.uk).

References

Ackerley, D., Booth, B. B. B., Knight, S. H. E., Highwood, E. J., Frame, D. J., Allen, M. R., & Rowell, D. P. (2011). Sensitivity of twentieth-century Sahel rainfall to sulfate aerosol and CO 2 forcing. *Journal of Climate*, *24*, 4999–5014. https://doi.org/10.1175/JCLI-D-11-00019.1

Adler, R. F., Huffman, G. J., Chang, A., Ferraro, R., Xie, P.-P., Janowiak, J., et al. (2003). The version-2 Global Precipitation Climatology Project (GPCP) monthly precipitation analysis (1979–present). *Journal of Hydrometeorology*, *4*(6), 1147–1167. https://doi.org/10.1175/1525-7541(2003)004<1147:TVGPCP>2.0.CO;2

Albrecht, B. A. (1989). Aerosols, cloud microphysics, and fractional cloudiness. *Science*, *245*, 1227–1230. https://doi.org/10.1126/science.245.4923.1227

Allen, M. R., & Stott, P. A. (2003). Estimating signal amplitudes in optimal fingerprinting, Part I: Theory. *Climate Dynamics*, *21*, 477–491. https://doi.org/10.1007/s00382-003-0313-9

Beck, C., Grieser, J., & Rudolf, B. (2005). A new monthly precipitation climatology for the global land areas for the period 1951 to 2000, *Climate Status Report 2004* (pp. 181–190). Offenbach, Germany: German Weather Service.

Biasutti, M. (2013). Forced Sahel rainfall trends in the CMIP5 archive. *Journal of Geophysical Research: Atmospheres*, *118*, 1613–1623. https://doi.org/10.1002/jgrd.50206

Bollasina, M. A., Ming, Y., & Ramaswamy, V. (2011). Anthropogenic aerosols and the weakening of the South Asian summer monsoon. *Science*, *334*(6055), 502–505. https://doi.org/10.1126/science.1204994

Bollasina, M. A., Ming, Y., Ramaswamy, V., Schwarzkopf, M. D., & Naik, V. (2014). Contribution of local and remote anthropogenic aerosols to the twentieth century weakening of the South Asian Monsoon. *Geophysical Research Letters*, *41*, 680–687. https://doi.org/10.1002/2013GL058183

Booth, B. B. B., Dunstone, N. J., Halloran, P. R., Andrews, T., & Bellouin, N. (2012). Aerosols implicated as a prime driver of twentieth-century North Atlantic climate variability. *Nature*, *484*(7393), 228–232. https://doi.org/10.1038/nature10946

Boucher, O., Randall, D., Artaxo, P., Bretherton, C., Feingold, G., Forster, P., et al. (2013). Clouds and aerosols. In T. F. Stockers et al. (Eds.), *Climate change 2013: The physical science basis Contribution Working Group I to Fifth Assessment Report of the Intergovernmental Panel on Climate Change* (pp. 571–657). Cambridge, United Kingdom and New York, NY, USA: Cambridge University Press.

Carslaw, K. S., Lee, L. A., Reddington, C. L., Pringle, K. J., Rap, A., Forster, P. M., et al. (2013). Large contribution of natural aerosols to uncertainty in indirect forcing. *Nature*, *503*(7474), 67–71. https://doi.org/10.1038/nature12674

Compo, G. P., Whitaker, J. S., Sardeshmukh, P. D., Matsui, N., Allan, R. J., Yin, X., et al. (2011). The twentieth century reanalysis project. *Quarterly Journal of the Royal Meteorological Society*, *137*, 1–28. https://doi.org/10.1002/qj.776

Cowan, T., & Cai, W. (2011). The impact of Asian and non-Asian anthropogenic aerosols on 20th century Asian summer monsoon. *Geophysical Research Letters*, *38*, L11703. https://doi.org/10.1029/2011GL047268

Dong, B., & Sutton, R. (2015). Dominant role of greenhouse-gas forcing in the recovery of Sahel rainfall. *Nature Climate Change*, *5*(August), 757–761. https://doi.org/10.1038/NCLIMATE2664

Dong, B., Sutton, R. T., Highwood, E., & Wilcox, L. (2014). The impacts of European and Asian anthropogenic sulfur dioxide emissions on Sahel rainfall. *Journal of Climate*, *27*(18), 7000–7017. https://doi.org/10.1175/JCLI-D-13-00769.1

Dong, B., Sutton, R. T., Highwood, E. J., & Wilcox, L. J. (2015). Preferred response of the East Asian summer monsoon to local and non-local anthropogenic sulphur dioxide emissions. *Climate Dynamics*, *46*(5), 1733–1751. https://doi.org/10.1007/s00382-015-2671-5

Dong, L., Zhou, T., & Chen, X. (2014). Changes of Pacific decadal variability in the twentieth century driven by internal variability, greenhouse gases, and aerosols. *Geophysical Research Letters*, *41*, 8570–8577. https://doi.org/10.1002/2014GL062269.Published

Donner, L. J., Wyman, B. L., Hemler, R. S., Horowitz, L. W., Ming, Y., Zhao, M., et al. (2011). The dynamical core, physical parameterizations, and basic simulation characteristics of the atmospheric component AM3 of the GFDL global coupled model CM3. *Journal of Climate*, *24*, 3484–3519. https://doi.org/10.1175/2011JCLI3955.1

Feudale, L., & Kucharski, F. (2013). A common mode of variability of African and Indian monsoon rainfall at decadal timescale. *Climate Dynamics*, *41*, 243–254. https://doi.org/10.1007/s00382-013-1827-4

Gallego, D., Ordóñez, P., Ribera, P., Peña-Ortiz, C., & García-Herrera, R. (2015). An instrumental index of the West African monsoon back to the nineteenth century. *Quarterly Journal of the Royal Meteorological Society*, *141*(October), 3166–3176. https://doi.org/10.1002/qj.2601

Ganguly, D., Rasch, P. J., Wang, H., & Yoon, J.-H. (2012). Climate response of the South Asian monsoon system to anthropogenic aerosols. *Journal of Geophysical Research*, *117*, D13209. https://doi.org/10.1029/2012JD017508

Guo, L., Turner, A. G., & Highwood, E. J. (2015). Impacts of 20th century aerosol emissions on the South Asian monsoon in the CMIP5 models. *Atmospheric Chemistry and Physics*, *15*, 6367–6378. https://doi.org/10.5194/acp-15-6367-2015

Guo, L., Turner, A. G., & Highwood, E. J. (2016). Local and remote impacts of aerosol species on Indian summer monsoon rainfall in a GCM. *Journal of Climate*, *29*, 6937–6955. https://doi.org/10.1175/JCLI-D-15-0728.1

Hannak, L., Knippertz, P., Fink, A. H., Kniffka, A., & Pante, G. (2017). Why do global climate models struggle to represent low-level clouds in the West African summer monsoon? *Journal of Climate*, *30*(5), 1665–1687. https://doi.org/10.1175/JCLI-D-16-0451.1

Hansen, J., Sato, M., Ruedy, R., Nazarenko, L., Lacis, A., Schmidt, G. A., et al. (2005). Efficacy of climate forcings. *Journal of Geophysical Research*, *110*, D18104. https://doi.org/10.1029/2005JD005776

Harris, I., Jones, P. D., Osborn, T. J., & Lister, D. H. (2014). Updated high-resolution grids of monthly climatic observations—The CRU TS3.10 dataset. *International Journal of Climatology*, *34*(3), 623–642. https://doi.org/10.1002/joc.3711

Held, I. M., Delworth, T. L., Lu, J., Findell, K. L., & Knutson, T. R. (2005). Simulation of Sahel drought in the 20th and 21st centuries. *Proceedings of the National Academy of Sciences of the United States of America*, *102*(50), 17,891–17,896. https://doi.org/10.1073/pnas.0509057102

Hsu, P., Li, T., & Wang, B. (2011). Trends in global monsoon area and precipitation over the past 30 years. *Geophysical Research Letters*, *38*, L08701. https://doi.org/10.1029/2011GL046893

Huang, J., Adams, A., Wang, C., & Zhang, C. (2009). Black carbon and West African monsoon precipitation: Observations and simulations. *Annales Geophysicae*, *27*, 4171–4181. https://doi.org/10.5194/angeo-27-4171-2009, 2009

Hwang, Y.-T., Frierson, D. M. W., & Kang, S. M. (2013). Anthropogenic sulfate aerosol and the southward shift of tropical precipitation in the late 20th century. *Geophysical Research Letters*, *40*, 2845–2850. https://doi.org/10.1002/grl.50502

Iles, C. E., & Hegerl, G. C. (2015). Systematic change in global patterns of streamflow following volcanic eruptions. *Nature Geoscience*, *8*(November), 838–844. https://doi.org/10.1038/NGEO2545

Iles, C. E., Hegerl, G. C., Schurer, A. P., & Zhang, X. (2013). The effect of volcanic eruptions on global precipitation. *Journal of Geophysical Research: Atmospheres*, *118*, 8770–8786. https://doi.org/10.1002/jgrd.50678

Ji, Z., Wang, G., Pal, J. S., & Yu, M. (2016). Potential climate effect of mineral aerosols over West Africa. Part I: Model validation and contemporary climate evaluation. *Climate Dynamics*, *46*(3), 1223–1239. https://doi.org/10.1007/s00382-015-2641-y

Kasoar, M., Voulgarakis, A., Lamarque, J.-F., Shindell, D. T., Bellouin, N., Collins, W. J., et al. (2016). Regional and global temperature response to anthropogenic SO_2 emissions from China in three climate models. *Atmospheric Chemistry and Physics*, *16*(2009), 9785–9804. https://doi.org/10.5194/acp-16-9785-2016

Kucharski, F., Zeng, N., & Kalnay, E. (2013). A further assessment of vegetation feedback on decadal Sahel rainfall variability. *Climate Dynamics*, *40*, 1453–1466. https://doi.org/10.1007/s00382-012-1397-x

Lamarque, J.-F., Bond, T. C., Eyring, V., Granier, C., Heil, A., Klimont, Z., et al. (2010). Historical (1850–2000) gridded anthropogenic and biomass burning emissions of reactive gases and aerosols: Methodology and application. *Atmospheric Chemistry and Physics*, *10*(15), 7017–7039. https://doi.org/10.5194/acp-10-7017-2010

Lau, K. M., Kim, M. K., & Kim, K. M. (2006). Asian summer monsoon anomalies induced by aerosol direct forcing: The role of the Tibetan Plateau. *Climate Dynamics*, *26*, 855–864. https://doi.org/10.1007/s00382-006-0114-z

Li, Z., Lau, W. K.-M., Ramanathan, V., Wu, G., Ding, Y., Manoj, M. G., et al. (2016). Aerosol and monsoon climate interactions over Asia. *Reviews of Geophysics*, *54*, 866–929. https://doi.org/10.1002/2015RG000500

Li, X., Ting, M., Li, C., & Henderson, N. (2015). Mechanisms of Asian summer monsoon changes in response to anthropogenic forcing in CMIP5 Models. *Journal of Climate*, *28*, 4107–4125. https://doi.org/10.1175/JCLI-D-14-00559.1

Martin, E. R., Thorncroft, C., & Booth, B. B. B. (2014). The multidecadal Atlantic SST–Sahel rainfall teleconnection in CMIP5 simulations. *Journal of Climate*, *27*(2), 784–806. https://doi.org/10.1175/JCLI-D-13-00242.1

Ming, Y., & Ramaswamy, V. (2009). Nonlinear climate and hydrological responses to aerosol effects. *Journal of Climate*, *22*(6), 1329–1339. https://doi.org/10.1175/2008JCLI2362.1

Nicholson, S. E. (2013). The West African Sahel: A review of recent studies on the rainfall regime and its interannual variability. *ISRN Meteorology*, *2013*, 453521. https://doi.org/10.1155/2013/453521

Philander, S. G. H., Gu, D., Halpern, D., Lambert, G., Lau, N.-C., Li, T., & Pacanowski, R. C. (1996). Why the ITCZ is mostly north of the equator. *Journal of Climate*, *9*(12), 2958–2972. https://doi.org/10.1175/1520-0442(1996)009<2958:WTIIMN>2.0.CO;2

Polson, D., Bollasina, M., Hegerl, G. C., & Wilcox, L. J. (2014). Decreased monsoon precipitation in the Northern Hemisphere due to anthropogenic aerosols. *Geophysical Research Letters*, *41*, 6023–6029. https://doi.org/10.1002/2014GL060811

Polson, D., Hegerl, G. C., Zhang, X., & Osborn, T. J. (2013). Causes of robust seasonal land precipitation changes. *Journal of Climate*, *26*(17), 6679–6697. https://doi.org/10.1175/JCLI-D-12-00474.1

Rotstayn, L. D., Collier, M. A., & Luo, J.-J. (2015). Effects of declining aerosols on projections of zonally averaged tropical precipitation. *Environmental Research Letters*, *10*(4), 44018. https://doi.org/10.1088/1748-9326/10/4/044018

Rotstayn, L. D., & Lohmann, U. (2002). Tropical rainfall trends and the indirect aerosol effect. *Journal of Climate*, *15*(15), 2103–2116. https://doi.org/10.1175/1520-0442(2002)015<2103:TRTATI>2.0.CO; 2

Salzmann, M., & Cherian, R. (2015). On the enhancement of the Indian summer monsoon drying by Pacific multidecadal variability during the latter half of the twentieth century. *Journal of Geophysical Research: Atmospheres*, *120*, 9103–9118. https://doi.org/10.1002/2015JD023313.Abstract

Salzmann, M., Weser, H., & Cherian, R. (2014). Robust response of Asian summer monsoon to anthropogenic aerosols in CMIP5 models. *Journal of Geophysical Research: Atmospheres*, *119*, 1–17. https://doi.org/10.1002/2014JD021783.1

Schneider, U., Becker, A., Finger, P., Meyer-Christoffer, A., Ziese, M., & Rudolf, B. (2014). GPCC's new land surface precipitation climatology based on quality-controlled in situ data and its role in quantifying the global water cycle. *Theoretical and Applied Climatology*, *115*, 15–40. https://doi.org/10.1007/s00704-013-0860-x

Schneider, T., Bischoff, T., & Haug, G. H. (2014). Migrations and dynamics of the intertropical convergence zone. *Nature*, *513*(7516), 45–53. https://doi.org/10.1038/nature13636

Sperber, K. R., Annamalai, H., Kang, I.-S., Kitoh, A., Moise, A., Turner, A., et al. (2013). The Asian summer monsoon: an intercomparison of CMIP5 vs. CMIP3 simulations of the late 20th century. *Climate Dynamics*, *41*, 2711–2744. https://doi.org/10.1007/s00382-012-1607-6

Takahashi, C., & Watanabe, M. (2016). Pacific trade winds accelerated by aerosol forcing over the past two decades. *Nature Climate Change*, *6*, 768–772. https://doi.org/10.1038/NCLIMATE2996

Taylor, K. E., Stouffer, R. J., & Meehl, G. A. (2012). An overview of CMIP5 and the experiment design. *Bulletin of the American Meteorological Society*, *93*(4), 485–498. https://doi.org/10.1175/BAMS-D-11-00094.1

Tett, S. F. B., Jones, G. S., Stott, P. A., Hill, D. C., Mitchell, J. F. B., Allen, M. R., et al. (2002). Estimation of natural and anthropogenic contributions to twentieth century temperature change. *Journal of Geophysical Research*, *107*(D16), 4306. https://doi.org/10.1029/2000JD000028

Ting, M., Kushnir, Y., Seager, R., & Li, C. (2009). Forced and internal twentieth-century SST trends in the North Atlantic. *Journal of Climate*, *22*(6), 1469–1481. https://doi.org/10.1175/2008JCLI2561.1

Tsai, I.-C., Wang, W.-C., Hsu, H.-H., & Lee, W.-L. (2016). Aerosol effects on summer monsoon over Asia during 1980s and 1990s. *Journal of Geophysical Research: Atmospheres*, *121*, 11,761–11,776. https://doi.org/10.1002/2016JD025388

Turner, A. G., & Annamalai, H. (2012). Climate change and the South Asian summer monsoon. *Nature Climate Change*, *2*(August), 587–595. https://doi.org/10.1038/nclimate1495

Twomey, S. (1977). The influence of pollution on the shortwave albedo of clouds. *Journal of the Atmospheric Sciences*, *34*, 1149–1152. https://doi.org/10.1175/1520-0469(1977)034<1149:TIOPOT>2.0.CO;2

Vuuren, D. P. V., Edmonds, J., Kainuma, M., Riahi, K., Nakicenovic, N., Smith, S. J., & Rose, S. K. (2011). The representative concentration pathways: An overview. *Climate Change*, *109*, 5–31. https://doi.org/10.1007/s10584-011-0148-z

Wang, B., Wu, R., & Lau, K.-M. (2001). Interannual variability of the Asian summer monsoon: Contrasts between the Indian and the Western North Pacific–East Asian monsoons. *Journal of Climate*, *14*, 4073–4090. https://doi.org/10.1175/1520-0442(2001)014<4073:IVOTAS>2.0.CO;2

Wang, H., Xie, S. P., & Liu, Q. (2016). Comparison of climate response to anthropogenic aerosol versus greenhouse gas forcing: Distinct patterns. *Journal of Climate*, *29*(14), 5175–5188. https://doi.org/10.1175/JCLI-D-16-0106.1

Wilcox, L. J., Highwood, E. J., Booth, B. B. B., & Carslaw, K. S. (2015). Quantifying sources of inter-model diversity in the cloud albedo effect. *Geophysical Research Letters*, *42*, 1568–1575. https://doi.org/10.1002/2015GL063301

Xie, S.-P., Lu, B., & Xiang, B. (2013). Similar spatial patterns of climate responses to aerosol and greenhouse gas changes. *Nature Geoscience*, *6*(10), 828–832. https://doi.org/10.1038/ngeo1931

Zelinka, M. D., Andrews, T., Forster, P. M., & Taylor, K. E. (2014). Quantifying components of aerosol-cloud-radiation interactions in climate models. *Journal of Geophysical Research: Atmospheres*, *119*, 7599–7615. https://doi.org/10.1002/2014JD021710